

Military Technical College,
Kobry El-Kobbah,
Cairo, Egypt



9th International Conference
On Aerospace Sciences &
Aviation Technology

INVESTIGATION OF FACTORS AFFECTING THE SHAPED CHARGE PERFORMANCE

By

Mohamed, S.Y.^{*}, Riad, A.M.^{*}, Kresha, Y.[#] and Ismail, M.M.^{*}

ABSTRACT

An analytical model has been developed to investigate the shaped charge phenomena. In this paper, the analytical model is only used to predict the influence of each shaped charge factor on jet penetration process through a metallic target. The main factors are: (i) liner thickness, (ii) liner material, (iii) cone angle, (iv) type of explosive, and (v) stand-off distance between the charge base and target surface.

An experimental program has been conducted to determine the effects of some shaped charge factors on its performance. These factors are: (a) liner material, (b) type of explosive, and (c) distance between charge base and target surface. Six shaped charges have been prepared and exploded at different distances from a steel target surface. For each tested shaped charge, the experimental measurements are concerned with the determination of the total depth of penetration and crater radius at the target surface.

For each shaped charge factor, both the measured depth of penetration and crater radius at the steel target surface are compared with the corresponding predicted results of the model. Moreover, representative samples of the model predictions concerning with the effect of each factor on the shaped charge performance, using the data of some tested shaped charges, are presented and discussed. The present results show that the depth of penetration increases with the increase of: (i) liner thickness up to a value of 0.05 the charge base diameter at short standoff distances, (ii) density of liner material at short standoff distances, (iii) power of used explosive, and (iv) standoff distance. In addition, the crater radius at the target surface increases with the increase of power of used explosives, and decreases with the increase of density of liner material at short standoff distances.

KEY WORDS

Explosive loading, Shaped charge phenomena, Explosive-metal interaction, Jet formation, and Jet penetration

* Egyptian Armed Forces.

Assoc. Prof., Head of R. & D. Dept., Helwan Industrial Eng. Company, Cairo, Egypt.

1. INTRODUCTION

The importance of civil and military applications of shaped charges pays the attention of many investigators to extensively study the shaped charge phenomena. Great efforts have been achieved to improve the shaped charge performance. Many investigators studied the effect of numerous factors of shaped charge on its performance. These factors are: (i) liner configuration, (ii) charge configuration, (iii) initiation mode, (iv) standoff distance, and (v) production techniques. The development of computer codes and high techniques for experimentation enriches this field. However, the use of analytical models is still regarded as the fast and cheap tool for fulfilling the design and optimization requirements put on shaped charges.

Murphy and Brown [1] studied numerically the effect of cone angle on jet formation process. Their predicted results showed that the small apex angle of a conical liner gave a fast tip velocity of a formed jet with a small jet mass. Moreover, Walter and Zukas [2] concluded that the liner with dual cone angle, biconic liner, could be used to produce a high velocity jet.

Chanteret and Lichtenberger [3] studied experimentally the effect of liner wall thickness on jet formation process. They concluded that the increase of liner thickness decreases the jet velocity and increases the velocity difference between successive break-up jet elements. Mayseless et al. [4] investigated the effect of liner thickness on jet formation by comparing their experimental results with that predicted analytically and numerically. They recommended that: (i) liner of thin wall produces a long jet with thick tip and thin uniform rear sections, (ii) the jet break-up time doesn't vary with liner thickness, (iii) the maximum jet penetration into a hard target at a long standoff distance is obtained when the liner thickness is less than 2% of the charge diameter.

The tapering of liner, i.e. thick wall of conical liner at its apex and thin wall at its base, allows the designer to control the jet velocity gradient, jet length and the break-up time of jet elements. Moreover, different liner contours have been developed; these have the tulip, trumpet and hemi-spherical shapes. The collapse of tulip and trumpet liners was similar to conical liners. The trumpet liner formed a jet with a high tip velocity and did not possess an inverse velocity gradient within its elements. The hemi-spherical liner exhibited an entirely different mode of collapse than the conical liner; it was inverted from the pole or turned inside out [2].

The influence of density of liner material on jet performance was investigated analytically by Chanteret [5]. He predicted that: (i) the increase in density of liner material decreased the jet tip velocity, and (ii) the total length of jet was proportional to the density of liner material of power 1/2 or 1/3. For continuous jet, he predicted that the doubling of density of liner material increased the depth of penetration by 12%. However, the depth of penetration was independent on the density of liner material for fully particulated jet.

Schwartz and Baker [6] showed that the liner fabrication had a strong influence on jet straightness. They carried out their experimental program to study the effect of liner surface finish on jet break-up. They found that the liner of rough surface finish exhibited quite brittle behaviour and the break-up time of the formed jet elements increased with increasing the surface roughness of liner.

Types of used explosives for shaped charges must have high densities and high detonation velocities. Simon [see Ref. [7]] found that the increase of explosive density and its specific energy resulted in a faster jet tip and retarded the break-up time of jet elements. Baker et al. [8] as well as Murphy et al. [9] determined experimentally that the use of powerful

explosives provided more detonation energies and resulted in: (i) long jet, (ii) great break-up time of formed jet elements, and (iii) great jet penetration depth into a target.

Jet formation and its performance through the target are affected by the geometry of the initial detonation wave front that incidents upon the shaped charge liner. The detonation wave shape and the associated pressure are strongly depended on the initiation method. The initiation could be central, end or multi-point as shown in Fig. 1. Elwani [10] carried out his experimental program to study the effect of different initiation methods on jet penetration into a target. He found that the maximum jet penetration was obtained with multi-point initiation method and attributed this to the convergent of detonation wave with the enhancement in detonation pressure being produced. Balche and Weimann [11] found that the stretching of jet could be increased by using the multi-point initiation method.

Standoff distance is an important factor affecting the shaped charge performance. This distance allows the formed jet to lengthen during its flight to the target. The increase in jet length is due to the velocity gradient between jet elements. The optimum standoff distance is a function of liner material, geometry of liner, pressure at detonation wave front and explosive configuration [10]. At optimum standoff distance, the formed continuous jet has its maximum length and a maximum penetration through the target is achieved.

In this paper, an analytical model has been developed to predict the influence of each shaped charge factor on its performance. The present model consists of three main phases; these are: (i) jet formation, (ii) jet break-up, and (iii) jet penetration phases. The governing equations of each phase are derived, arranged and compiled into a computer program. An experimental program has been conducted to study the effect of some shaped charge factors on its performance. Six shaped charges, having different explosives and liner materials, are prepared and exploded at different standoff distances from a steel target. The effect of each factor is evaluated by comparing the measured depth of jet penetration and the crater radius at the target surface with the corresponding predicted values of the present model. Moreover, representative samples of model predictions showing the effect of each non-tested shaped charge factor on its performance are presented and discussed.

2. ANALYTICAL MODELLING

The present work investigates the influence of shaped charge factors on its performance using the one-dimensional analytical model developed by Mohamed [12]. This model is divided into three main phases; these are: (i) jet formation, (ii) jet break-up, and (iii) jet penetration phases. For each phase, the shaped charge liner or formed jet is divided into n elements. Figure 2 presents a schematic drawing of a collapsed liner element during jet formation phase. In this model, the governing equations representing the deflection angle, collapse angle, real collapse velocity, jet velocity and jet mass associated with each collapsed element of liner are derived. For jet break-up phase, a recent formula, developed by Hennequin [13], is selected to predict the break-up time of each jet element. This formula is put on its final form based on the results of other investigators.

The modeling of jet penetration into a target is based on the modified Bernoulli's equation which incorporates the strength terms of jet and target materials, respectively. Moreover, the compression in jet length during its penetration through the target is included in the analysis. A schematic drawing representing the jet penetration into a target can be shown in Fig. 3. Equations representing the initial length of formed jet, the jet length prior to impact are derived. In addition, The main equations predicting the penetration velocity, penetration depth and radius of crater at the target surface associated with each

penetrated element of jet are also derived. The total depth of penetration for a particulated jet can be predicted by the present model.

In the following, the governing equations representing each phase of the analytical model are presented. The interested reader could be referred to the original reference for further details [12].

2.1. Governing Equations of Jet Formation Phase

- a) The real collapse velocity, V_{real} , as a function of the time at which each collapsed liner element reaches the charge axis, t_r , is represented by:

$$V_{real} = V_o [1 - e^{-(t_r - t_o)/\tau}], \quad (1)$$

where V_o is the gurney velocity, velocity imparted to a metal incontact with a detonating explosive, t_o is the time taken by the detonation wave front to reach the liner element, and τ is time constant. The gurney velocity as a function of the ratio of mass of liner element to the mass of explosive above this element, μ , is represented by [2]:

$$V_o = 1.2U_D \left[\frac{\sqrt{1 + 32/(27\mu)} + 1}{\sqrt{1 + 32/(27\mu)} - 1} \right], \quad (1a)$$

where U_D is the detonation velocity of the used explosive. The time constant, τ , is represented by [14]:

$$\tau = m_{Li} V_o / P_{cj}, \quad (1b)$$

and

$$P_{cj} = 0.25 \rho_{exp} U_D^2. \quad (1c)$$

where m_{Li} is the mass of the liner element per its lateral area, P_{cj} is the Chapman-Jouguet pressure, and ρ_{exp} is the density of explosive material.

- b) The deflection angle δ of each collapsed liner element is represented by:

$$\delta = \sin^{-1}(V_{real} \cos \alpha / 2U_D), \quad (2)$$

where α is the half of the cone apex angle.

- c) The collapse angle β associated with each collapsed liner element is determined by [15]:

$$\beta = (\beta^* + \Delta\beta), \quad (3)$$

and

$$\beta^* = \alpha + 2\delta. \quad (3a)$$

where β^* is the collapse angle obtained by steady state theory [2]. The angle $\Delta\beta$ is determined using the following equation [15]:

$$\Delta\beta = \tan^{-1} \left[-X_l \sin \alpha / [\cos(\alpha + \delta) \cos \delta] \right] (V'_{real} / V_{real}), \quad (3b)$$

where V_{real} is the real collapse velocity of each liner element, and V'_{real} is the partial derivative of the real collapse velocity with respect to the distance of the liner element from the liner apex; this partial derivative is determined using the following equation:

$$V_{real} = (dV_o/d\mu)*(d\mu/dX_i) * [1 - e^{-(t-t_o)/\tau}] \quad (3)c$$

d) The velocity of jet generated from each collapsed element of liner, V_j , is represented by:

$$V_j = V_{real} * \text{cosec}(\beta/2) * \cos(\alpha + \delta - (\beta/2)) \quad (4)$$

e) The mass of jet generated from each collapsed element of liner, m_{ji} , is represented by [2]:

$$m_{ji} = M_{L_i} * \sin^2(\beta/2) \quad (5)$$

where M_{L_i} is the mass of collapsed element of liner.

2.2. Governing Equations of Break-up Phase

The break-up time of each jet element, t_{bi} , is determined using the semi-empirical formula developed by Hennequin [13]. The selected formula in its final form is represented by:

$$t_{bi} = 2.92 (r_{ji} / V_{pl}) + 0.46 (L_i / V_{pl}), \quad (6)$$

where r_{ji} is the initial radius of each jet element, V_{pl} is the velocity difference between the jet particulated elements, and L_i is the length of the particulated jet element. The velocity difference between particulated jet elements is represented by [16]:

$$V_{pl} = (V_{tip} - V_{tail}) / n_r, \quad (6)a$$

where V_{tip} is the velocity of front element of jet, V_{tail} is the velocity of rear element of jet, and n_r is the number of elements resulted from the jet break-up.

2.3. Governing Equations of Jet Penetration Phase

a) The total initial length of jet at the end of liner collapse process is represented by:

$$L_{jt} = L_{j1} + L_{j2} \quad (7)$$

where L_{j1} is the initial length of jet for the elements which have an inverse velocity gradient in between; the number of these elements is taken to be equal to (p-1) elements, and L_{j2} is the initial length of jet for the elements which have a velocity gradient in between; their number is taken to be equal to (n-p) elements. The initial jet length of the (p-1) elements is represented by:

$$L_{j1} = \sum_{i=1}^{p-1} l_{1i} + \sum_{i=1}^{p-1} (V_1 - V_{i+1}) * \Delta t_i, \quad (7)a$$

where l_{1i} is the length of each element of liner from the (p-1) elements, V_1 is the velocity of jet associated with the first element of collapsed liner, V_{i+1} is the jet velocity associated with the subsequent elements of collapsed liner, Δt_i is the difference between the arrival times of two successive elements to the cone axis. The initial jet length of the (n-p) elements is represented by:

$$L_{j2} = \sum_{i=p}^n l_{2i} + \sum_{i=p}^n (V_{max} - V_{i+1}) * \Delta t_i, \quad (7)b$$

where l_{2i} is the length of each element of liner from the (n-p) elements, V_{max} is the maximum velocity of jet, V_{i+1} is the jet velocity associated with the subsequent elements of collapsed liner.

b) The final length of jet prior to impact, L_{jt} , is determined by:

$$L_{jt} = L_{jl} + (V_{tip} - V_{tail}) * T_{bz} \quad (8)$$

where T_{bz} is the traveling time of the jet to cover the distance S_D , distance between the front of initial length of jet and target surface. The time, T_{bz} , is determined by:

$$T_{bz} = S_D / (V_{tip}) \quad (8)a$$

For particulated jet, the reader could be referred to the original reference to know the sequence of determining the length of jet prior to impact [12].

c) The cumulative length of jet, L_{jcum} , is determined by:

$$L_{jcum} = L_{jt} + (V_{tip} - V_{tail}) * t_{b1} \quad (9)$$

where t_{b1} is the time at which the first element of jet is broken-up.

d) The interface pressure, P_i , between the penetrated jet element and target is represented by [17]:

$$P_i = \lambda \rho_j (V_i - U_i)^2 = \rho_t U_i^2 + 2\sigma \quad (10)$$

and

$$\sigma = \sigma_t - \sigma_j \quad (10)a$$

where λ is constant which is equal to one for a continuous jet and less than one for a particulated jet [17], ρ_j is the density of jet material, V_i is the velocity of jet penetrated element, U_i is the penetration velocity, ρ_t is the density of target material, σ_t is the resistance factor of target material, and σ_j is the resistance factor of jet material.

e) The penetration velocity for each penetrated jet element is represented by:

$$U_i = \frac{V_i - \sqrt{\varphi V_i^2 + A_t (1 - \varphi)}}{(1 - \varphi)} \quad (11)$$

where

$$\varphi = \frac{\rho_t}{\lambda \rho_j} \quad \text{and} \quad A_t = \frac{2\sigma}{\lambda \rho_j} \quad (11)a$$

f) The decreasing rate of length of jet penetrating element, L_{jft} , is:

$$\frac{dL_{jft}}{dt} = - (V_i - U_i) \quad (12)$$

g) The rate of change of penetration depth for each penetrated element of jet, Z_i , is:

$$\frac{dZ_i}{dt} = U_i \quad (13)$$

h) The compressed length of jet during the penetration of the interacting element of jet with the target is represented by:

$$L_c = ((V_i - U_i) - V_{tail}) * \Delta t, \quad (14)$$

where L_c is the decrease in jet length due to its compression.

i) For a particulated jet, the depth of penetration into a target, Z' , is calculated using the following equation [11]:

$$Z' = Z \left(1 - \frac{g}{g_o} \right), \quad (15)$$

where Z is the total depth of penetration of continuous jet, g is the sum of gap distances between the break-up jet elements ($=\Sigma g_i$), and g_o is an empirical constant. For each break-up jet element, the gap distance g_i is calculated using the following equation:

$$g_i = (V_i - V_{i+1}) * (T_{bz} - t_{bi}). \quad (15a)$$

j) The crater radius, r_c , as a function of time, t , is determined by:

$$r_c = \sqrt{\frac{A}{B} - \left(\sqrt{\frac{A}{B} - r_{ji}^2} - t_c \sqrt{B} \right)^2}, \quad (16)$$

where

$$A = \frac{2r_{ji}^2 p_i}{\rho_t}, B = 2 \frac{\sigma_t}{\rho_t}. \quad (16a)$$

k) The radius of the penetrated jet element r_{ji} is determined using the following equation:

$$r_{ji} = \sqrt{\frac{m_{ji}}{\pi L_{ji} \rho_j}}, \quad (17)$$

where m_{ji} is the mass of penetrated jet element, and L_{ji} is the length of the penetrated element of jet.

The governing equations of each phase, of the analytical model that describes the shaped charge phenomena, have been introduced. All equations are arranged and compiled into a computer program. The input data to the program are easily determined. In the following, the predicted results of the present model are essentially concerned with studying the effect of each shaped charge factor on its performance.

3. EXPERIMENTAL WORK

The main objective of experimental work was to assess the predictions of the present model. The experimental facilities of the shaped charge laboratory, Explosives Dept., MTC, were used to prepare six small size shaped charges with different high explosives and liner materials. Each prepared charge was designated by letters and number (e.g. charge no. 1 is designated by Ch1). Figure 4 shows a schematic drawing of a prepared shaped charge. The data of each prepared shaped charge are listed in Table 1. For space limitation, the interested reader could be referred to the original reference for further details [12].

The target material is selected to be steel. The characterization of the steel target had been performed in the Dept. of Research and Development, Helwan Engineering Industrial Company (Formerly MF No. 99), Helwan, Cairo. The target characterization includes: (i) chemical analysis, (ii) measurement of hardness and using conversion tables to determine the target strength. The chemical composition of the ingredients of target material was determined using a Direct Emission Spectrometer Analyzer named Polyvac-E982; two specimens were used to perform this test. In addition, three specimens were prepared and the hardness was measured using a Rockwell Hardness Tester, Model Indentec. The hardness was measured at different points on the surface of each specimen.

The ballistic tests of the prepared shaped charges were carried out in the shaped charge laboratory, Explosives Dept., MTC. The ballistic set-up consists mainly of: (i) detonation chamber, (ii) fire control device, (iii) prepared shaped charge, and (iv) steel target plates. A photograph of the ballistic set-up can be shown in Fig. 5. For each tested shaped charge, the ballistic measurements were mainly concerned with the determination of the depth of jet penetration into a steel target and the crater radius at the target surface. The ballistic measurements were carried out in Helwan Engineering Industrial Company. The penetrated steel plates were cut using EDM wire cutting technique. For each tested shaped charge, X-ray technique was used to determine the aforementioned ballistic measurements.

4. RESULTS AND DISCUSSIONS

In the following, the present results are classified into: (i) results of target material characterization, (ii) comparison of the current experimental results with model predictions, (iii) comparison between predicted and experimental results for the tested shaped charge factors, and (iv) predictions of the effect of non-tested shaped charge factors on shaped charge performance. The tested shaped charge factors are: (a) density of liner material, (b) type of explosive, and (c) standoff distance whereas, the non-tested shaped charge factors are: (a) cone angle, and (b) thickness of liner wall. Both the depth of penetration and crater radius associated with the change of each shaped charge factor at different standoff distances are used to evaluate the effect of non-tested shaped factors on shaped charge performance.

4.1. Results of Target Material Characterization

The chemical composition of the ingredients of the steel target is listed in Table 2. Moreover, the mean of the measured values of target hardness is 41.5 Rc. The corresponding tensile strength determined from the conversion tables is 1400 MPa.

Table 1. Data of prepared and tested shaped charges [12].

Charge Design.	Base Dia., D_B [mm]	Cone Angle, 2α [°]	Cone Mat.	Liner Density, ρ_L [g/cm ³]	Liner Thick., T_L [mm]	Expl. Type	Expl. Density, ρ_{exp} [g/cm ³]	Dist., S [mm]
Ch1	14.9	60	Al.	2.6	0.8	RDX	1.77	15
Ch2	14.9	60	Cu	8.9	0.8	HMX	1.89	15
Ch3	14.9	60	Cu	8.9	0.8	TNT	1.54	15
Ch4	14.9	60	Cu	8.9	0.8	RDX	1.77	15
Ch5	14.9	60	Cu	8.9	0.8	RDX	1.77	30
Ch6	14.9	60	Cu	8.9	0.8	RDX	1.77	45

4.2. Comparison of Current Experimental Results with Model Predictions

The prepared charges during the experimental work are exploded at different distances from a steel target. For each shaped charge, both the jet penetration depth and the crater entrance radius are measured. Table 3 lists the experimental measurements due to explosion of the prepared charges and the corresponding predicted results of the present model.

The predicted values of penetration depth are compared with the corresponding experimental measurements; good agreement is generally obtained. Moreover, it is found that the maximum error is 17.4% for the charge Ch4. The obtained errors between predicted and experimental results can be attributed to the following: (i) the neglect of the charge height behind the cone apex angle, (ii) the neglect of the effect of charge confinement, and (iii) the after flow residual jet penetration. The suggested reasons of errors are difficult to be represented in the present analytical model.

The predicted results of crater radii are far from the corresponding experimental measurements. An additional analytical investigation is needed to suit a better agreement between the model predictions and experimental measurements. The trend of the current predicted results is similar to that obtained by Held [18] who concluded that (i) the predicted crater radii be generally greater than the corresponding measured ones, and (ii) an extensively analytical study is needed to develop a model capable of predicting a crater radius close to experimental measurement.

4.3. Comparison Between Predicted and Experimental Results for the Tested Shaped Charge Factors

4.3.1. Density of liner material

The effect of liner density on jet penetration depth is studied using the charges Ch1 and Ch4. The predicted change of penetration depth with liner density is plotted in Fig. 6. The corresponding measured penetration depths are also depicted on the same figure. It is shown from the figure that the depth of penetration increases with liner density. Moreover, the predicted results of the model are in good agreement with the corresponding measured ones at different liner densities. The maximum difference between the predicted and measured depths of penetration is 15.7% at the lowest liner density. The present trends for the change of penetration depth with liner density are similar to that obtained by Cowan et al. [19].

Table 2. Chemical composition of steel target in percent.

Element	Fe	C	Si	Mn	Ni	Al	Cu	Cr	Mo	Others
Percent	96.2	0.12	1.57	1.29	0.066	0.044	0.093	0.19	0.18	0.247

Table 3. Predicted and measured depth of penetration and crater radius for each used charge.

Charge Designa.	Penetration depth [mm]		Crater entrance radius [mm]	
	Predicted	Measured	Predicted	Measured
Ch1	16	19	14	5
Ch2	22	26	8.8	4
Ch3	16	19	6	3
Ch4	19	23	6	3.7
Ch5	35	34	4.2	3.5
Ch6	46	42	3.6	3

The predicted change of crater entrance radius with the liner density using the charges Ch1 and Ch4 is plotted in Fig. 7. The corresponding experimental measurements are depicted on the same figure. The figure shows that the crater radius decreases with the increase of liner density. For each liner material, the difference between predicted and experimental results assesses the need of extensively analytical study to improve the predictive capability of the derived formula determining the crater radius.

4.3.2. Type of explosive

The explosive power increases with the increase of explosive density and its detonation velocity. The data of the charges Ch2, Ch3 and Ch4 listed in Table 1 are fed into the model to study the effect of explosive type on shaped charge performance. Figure 8 plots the predicted and experimental changes of penetration depth with explosive type (types of explosive are in ascending order according to their power). It is seen from the figure that the depth of penetration increases with the increase of explosive power. Moreover, good agreement is obtained between the predicted depth of penetration and the corresponding experimental measurements for the different explosive powers; the maximum difference is 17.4% for the RDX explosive charge. Similar trends to the predicted change of penetration depth with explosive type using the present model are obtained by Baker et al. [8].

The predicted and experimental changes of crater entrance radius with the explosive type are plotted in figure 9. It is seen from figure that the crater radius increases with the increase of explosive power. In addition, a great difference is obtained between the predicted and experimental results for the different type of explosive. The present results prove the necessity of extensively analytical study to derive a formula has a good predictive capability of crater radius.

4.3.3. Standoff distance

The effect of standoff distance, between the charge base and target surface, on jet penetration depth and crater radius is studied using the charges Ch4, Ch5 and Ch6. The predicted change of penetration depth with standoff distance is plotted in Fig. 10; the corresponding experimental measurements are depicted on the same figure. The figure

shows that the depth of penetration increases with the increase of standoff distance. In addition, good agreement is obtained between the predicted depth of penetration and experimental measurements at different standoff distances. The trends of the present results are similar to that obtained by Schwartz et al. [20] and Teng et al. [21].

The predicted and experimental changes of crater radius with standoff distance are depicted on Fig. 11. The crater radius is noticed to be decreased with the increase of standoff distance. This is attributed to the stretching of jet length prior to impact and the decrease in radius of penetrated jet element due to jet stretching. With the increase of standoff distance, the predicted crater radii seem to be close to the corresponding measured values.

4.4. Predictions of the Effect of Non-Tested Shaped Charge Factors on its Performance

4.4.1. Cone angle

In the following, the effect of cone angle on shaped charge performance is studied. The data of the charge No. 4, Ch4, listed in Table 1 is fed into the model with the change of the half cone angle, α , three times; the input values of the angles are 20°, 25° and 30°, respectively. Figure 12 plots the change of penetration depth with half cone angle at different standoff distances. It is seen from the figure that the depth of penetration decreases with the increase of half cone angle at short standoff distances. This is attributed to the decrease of jet velocity with the increase of half cone angle. However, the depth of penetration does not much vary with the half cone angles of 25° and 30° at large standoff distance. Therefore, the defeat of metallic armours at short standoff distances is attained by liners having small cone angles. More experimentation is needed to determine the limit of cone angle at which the maximum depth of penetration is obtained.

The change of crater radius with half cone angles at different standoff distances is plotted in Fig. 13. Similar trends at different standoff distances are predicted; it increases with the decrease of half cone angle. This is attributed to the decrease of jet velocity with the increase of half cone angle.

4.4.2. Thickness of liner wall

The effect of liner wall thickness on shaped charge performance is also studied. The data of the charge No. 1, Ch1, listed in Table 1 is fed into the model with the change of the wall thickness, T_L , three times; the input values of the liner wall thickness are 0.4, 0.8, and 1.2 mm, respectively. Figure 14 plots the change of penetration depth with liner wall thickness at different standoff distances. It is noticed from the figure that the liner of wall thickness 0.4 mm predicts a deeper penetration than that of the other wall thicknesses of liner at large standoff distances; the lowest depth is associated with a wall thickness of 1.2 mm.

Mayseless et al. [4] predicted that the depth of penetration increases with the increase of liner thickness up to a limit value of thickness beyond which the depth of penetration decreases. The present results show that the liner wall thickness of 0.8 mm predicts the maximum depth of penetration at short standoff distances, this wall thickness is equivalent to 5% of the charge base diameter. Mayseless et al. determined that the maximum depth of penetration was associated with a liner thickness of 2% of the charge base diameter (= 81.3 mm). The predicted results of the present model prove its predictive capabilities for depth of jet penetration through the target.

The predicted change of crater radius with liner wall thickness at different standoff distances is plotted in Fig. 15. The crater entrance radius increases with wall thickness at the different standoff distances. This is attributed to the increase of jet mass and the diameter of its tip with the increase of liner wall thickness. Moreover, for the application of shaped charge to perform a wider crater with small depth of penetration, liners of thick wall are recommended.

5. CONCLUSIONS

An analytical model has been developed to investigate the influence of shaped charge factors on its performance. Moreover, an experimental program has been carried out to assess the predictions of the model. The predicted depths of penetration and crater radii at the target surface are compared with the corresponding experimental measurements of the tested shaped charges. Good agreement is obtained for the depth of penetration; however, further analytical study is needed to improve the predictive capability of the model for crater radius.

Analysis of the present results for the factors affecting the shaped charge performance results in:

- i) Liners of small cone angles achieve deeper penetration into metallic targets at short standoff distances whereas, the depth of penetration does not much vary with the increase of cone angle at large standoff distances.
- ii) The maximum depth of penetration is predicted when the liner wall thickness has a value of 0.05 the charge base diameter at short standoff distances. Further experimentation is needed to prove this result.
- iii) The increase of the density of liner material results in a deeper penetration into metallic target with a corresponding decrease in crater radius.
- iv) The penetration depth increases with the standoff distance. Moreover, the jet attains its deepest penetration at a distance named optimum standoff distance.
- v) A wider crater with deeper penetration is attained with a more powerful explosive.
- vi) The present model can be successfully extended to model other shaped charge configurations and to optimize their design features.

6. REFERENCES

1. M. J. Murphy, M. J. and Brown, R. E., "On the Utility of the Finite Element Method For Shaped Charge Design", Computational Plasticity Models, Software and Applications, editors: D. R. Hinton and E. Onate, Pintridge Press, U.K. (1987).
2. Walters, P. and Zukas, J. A., "Fundamentals of Shaped Charges", Wiley Interscience Publication, John Wiley and Sons, New York, U.S.A. (1989).
3. Chanteret, P. Y. and Lichtenberger, A., "About Varying Shaped Charge Liner Thickness", 17th Int. Symp. on Ballistics, Midrand, South Africa, 23-27 March 1998.
4. Mayseless, M., Hirsch, E., Lindenfield, A. and Bar Me, "Jet Tip and Appendix Dependence on Liner Thickness in 60° Point Initiated Shaped Charge", 17th Int. Symp. on Ballistics, Midrand, South Africa, 23-27 March 1998.
5. Chanteret, P. Y., "Theoretical Considerations About Jet Density and Shaped Charge Performance", 17th Int. Symp. on Ballistics, Midrand, South Africa, 23-27 March 1998.
6. Schwartz, A. and Baker E., "Effect of Interior Surface Finish on the Break-up of Copper Shaped Charge Jet", 18th Int. Symp. on Ballistics, San Antonio, 15-19 November 1999.

7. Mayselless, M., Hirsch, E., Lindenfeld, A. and Shwartz, A., "Effect of Explosive Energy on the Shaped Charge Jet Formation Characteristics", 16th Int. Symp. on Ballistics, San Francisco, USA, September 23-28, 1996.
8. Baker, E., Daniels, A., Fuchs, B., Nicolich, S., Orosz, J., Pham, J., Travers, B. and Vuong, T., "Improved Performance of Shaped Charge Warheads Using More Powerful Explosive Formulations", 17th Int. Symp. on Ballistics, Midrand, South Africa, 23-27 March 1998.
9. Murphy, M., Baum, D., Simpson, R., Monolo, J., Motesi, L., Newman, K., Tuerpe, D. and Osborn, J., "Demonstration of Enhanced Warhead Performance with More Powerful Explosives", 17th Int. Symp. on Ballistics, Midrand, South Africa, 23-27 March 1998.
10. Elwani, H., "The Use of Polymer Bonded Explosives in Improved Linear Shaped Charge Designs", Ph. D. Thesis, Cranfield University, U.K. (1994).
11. Blache, A. and Weimann, K., "Generation of Different Detonation Wave Contours", 16th Int. Symp. on Ballistics, San Francisco, USA, September 23-28, 1996.
12. Mohamed, S. Y., "Factors Affecting the Shaped Charge Performance", M. Sc. Thesis, M.T.C., Cairo, Egypt (2000).
13. Hennequin, E., "Modeling of Shaped Charge Jet Break-up", Propellants, Explosives, Pyrotechnics Vol. 21, pp. 181-185 (1996).
14. Battacharya, R., Singh, S., Kishore, P., Raychaudhuri, T. K. and Sharma, V. K., "A Simplified Approach for Development of One-Dimensional Time Dependent PC Based Code for Shaped Charge Design", 16th Int. Symp. On Ballistics, San Francisco, CA, USA, September 1996.
15. Liu Gui-Xi, "The Simplified Model for Predicting Shaped Charge Jet Parameters", Propellants, Explosives, Pyrotechnics, Vol. 20, pp. 279-282 (1995).
16. Chanteret, P.Y., "Considerations about the Analytical Modeling of Shaped Charges", Propellants, Explosives, Pyrotechnics, Vol. 18, pp. 337-344 (1993).
17. Walters, W., Flis, W. S. and Chou, P. C., "A Survey of Shaped-Charge Jet Penetration Models", Int. J. Impact Engng., Vol. 7, No 3, pp. 307-325 (1988).
18. Held, M., "Verification of the Equation for Radial Crater Growth by Shaped Charge Jet Penetration", Int. J. Impact Engng., Vol. 17, pp. 387-398 (1995).
19. Cowan, K. G., Mawella, K. J., Standing, D. J., Bourne, B., Jones, J. and Kitney, A., "Analytical Code and Hydrocode Modelling and Experimental Characterisation of Shaped Charges Containing Tungsten Liners", 17th Int. Symp. on Ballistics, Midrand, South Africa, 23-27 March 1998.
20. Schwartz, A., Minich, R. and Baker, E., "Statistical Analysis of the Particulation of Shaped Charge Jets", 18th Int. Symp. on Ballistics, San Antonio, 15-19 November 1999.
21. Teng, T., Lin, C. and Hung C., "Simulation and Experiment of Cutting Effect for Linear Shaped Charge", 18th Int. Symp. on Ballistics, San Antonio, 15-19 November 1999.

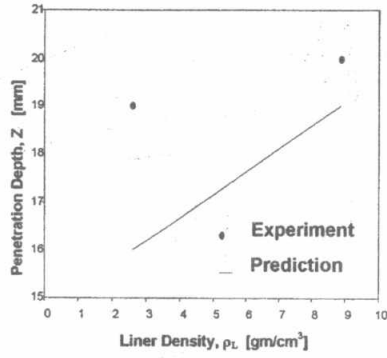


Fig. 6. Predicted and experimental changes of penetration depth with liner density.

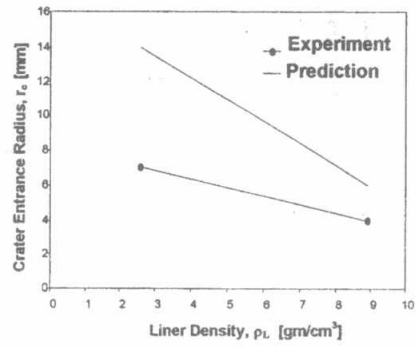


Fig. 7. Predicted and experimental changes of crater entrance radius with liner density.

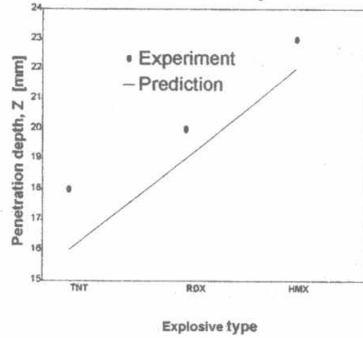


Fig. 8. Predicted and experimental changes of penetration depth with explosive type.

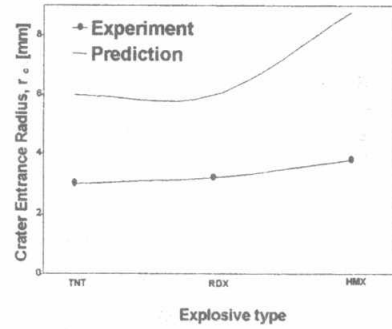


Fig. 9. Predicted and experimental changes of crater entrance radius with explosive type.

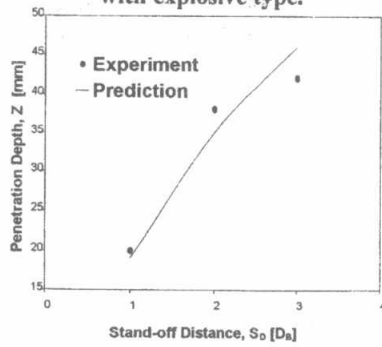


Fig. 10. Predicted and experimental changes of penetration depth with standoff distance.

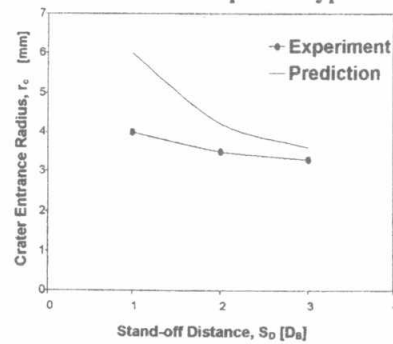


Fig. 11. Predicted and experimental changes of crater entrance radius with standoff distance.

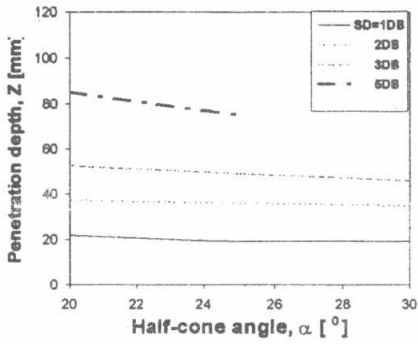


Fig. 12. The predicted change of penetration depth with half cone angle at different standoff distances.

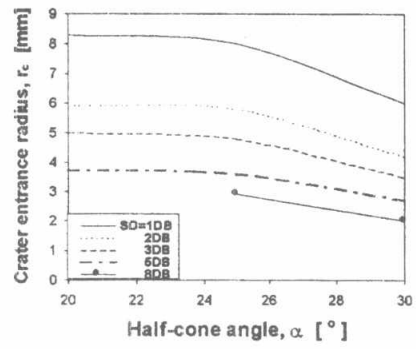


Fig. 13. The predicted change of crater entrance radius with half cone angle at different standoff distances.

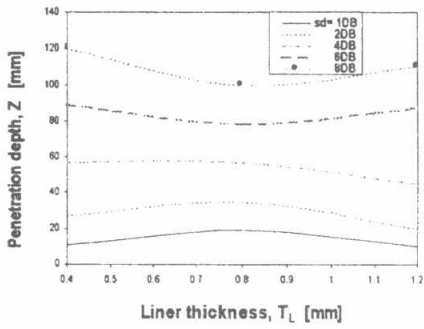


Fig. 14. The predicted change of penetration depth with liner wall thickness at different standoff distances.

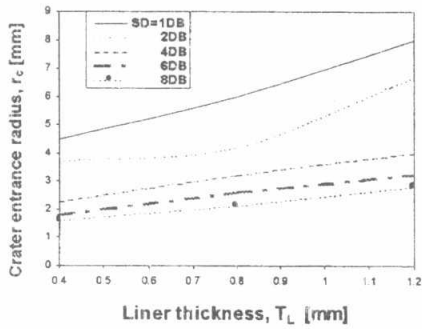


Fig. 15. The predicted change of crater entrance radius with liner wall thickness at different standoff distances.